Promotional Effect of Cerium and/or Zirconium Doping on Cu/ZSM-5 Catalysts for Selective Catalytic Reduction of NO by NH$_3$

Ye Liu, Chonglin Song *, Gang Lv, Chenyang Fan and Xiaodong Li

State Key Laboratory of Engines, Tianjin University, Tianjin 300072, China; liuyeskle@tju.edu.cn (Y.L.); lvg@tju.edu.cn (G.L.); fanchenyang@tju.edu.cn (C.F.); linahaifeng@tju.edu.cn (X.L.)

* Correspondence: songchonglin@tju.edu.cn; Tel.: +86-22-27406840-8020

Abstract: The cerium and/or zirconium-doped Cu/ZSM-5 catalysts (CuCe$_x$Zr$_{1-x}$O$_y$/ZSM-5) were prepared by ion exchange and characterized by X-ray diffraction (XRD), transmission electron microscopy (TEM), X-ray photoelectron spectroscopy (XPS), temperature-programmed reduction by hydrogen (H$_2$-TPR). Activities of the catalysts obtained on the selective catalytic reduction (SCR) of nitric oxide (NO) by ammonia were measured using temperature programmed reactions. Among all the catalysts tested, the CuCe$_{0.75}$Zr$_{0.25}$O$_y$/ZSM-5 catalyst presented the highest catalytic activity for the removal of NO, corresponding to the broadest active window of 175–468 °C. The cerium and zirconium addition enhanced the activity of catalysts, and the cerium-rich catalysts exhibited more excellent SCR activities as compared to the zirconium-rich catalysts. XRD and TEM results indicated that zirconium additions improved the copper dispersion and prevented copper crystallization. According to XPS and H$_2$-TPR analysis, copper species were enriched on the ZSM-5 grain surfaces, and part of the copper ions were incorporated into the zirconium and/or cerium lattice. The strong interaction between copper species and cerium/zirconium improved the redox abilities of catalysts. Furthermore, the introduction of zirconium abates N$_2$O formation in the tested temperature range.

Keywords: selective catalytic reduction; nitric oxide; ammonia; Cu/ZSM-5; cerium; zirconium

1. Introduction

Metal-based ZSM-5 catalyst has received considerable attention due to its excellent performance in the low-temperature selective catalytic reduction (SCR) reaction [1–4]. As a crystalline inorganic polymer, ZSM-5 consists of a three-dimensional network of SiO$_4$ and AlO$_4$ tetrahedra linked by interconnecting oxygen ions. When transition metal is introduced in ZSM-5, the catalytic performance can be enhanced through different types of active species, including isolated ions on the exchange sites within the ZSM-5 structure, metal oxide clusters, and metal oxide particles in the appearance of ZSM-5 [5,6]. Among all the relevant catalysts studied, Cu/ZSM-5 is of particular interest because it exhibits excellent SCR activity in NO abatement [7,8]. However, it has been reported that the catalytic activity of Cu/ZSM-5 catalysts is decreased, after an initial increase, with increasing copper content [8], which suggests that it is difficult to improve catalytic performance by merely increasing the copper content.

Fabrication of copper catalysts can be implemented through incorporating more reducible promoters, such as ceria, lanthana, and zirconia [2,9,10]. Cerium-containing materials are promising candidates for the application of NO abatement due to their high oxygen storage capacity and unique redox properties [11,12]. Nevertheless, a major drawback of cerium lies in its poor thermal and hydrothermal stability, especially under a practical diesel exhaust atmosphere [11,13]. It is well known

that the incorporation of zirconia in cerium-based materials via high-temperature calcination can enhance the thermal stability and dispersion of the active component on the support surface [13,14]. Furthermore, the addition of zirconia to ceria introduces structural defects through substitution of Ce^{4+} by Zr^{4+}, which further enhances the oxygen storage capacity of ceria, the oxygen mobility in the lattice, the redox property, and thermal resistance [9,11,13]. Consequently, cerium and zirconium materials have the potential to improve the catalytic activity of Cu/ZSM-5 catalyst. Based on this background, the present work attempts to address the effects of the cerium and/or zirconium addition on Cu/ZSM-5 catalysts for SCR of NO by NH_3. A series of $CuCe_xZr_{1-x}O_y$/ZSM-5 catalysts (x = 0, 0.25, 0.50, 0.75 and 1) were synthesized using a conventional ion-exchange method, and the effects of adding cerium/zirconium metal ions into Cu/ZSM-5 catalysts on the SCR reaction were investigated using X-ray diffraction (XRD), transmission electron microscopy (TEM), X-ray photoelectron spectroscopy (XPS), and temperature-programmed reduction by hydrogen (H_2-TPR). The correlation between the structural characteristics, dispersion, reduction, and activity for the SCR process are discussed. The purpose of this work is to establish the relationships between structure and catalytic performance, which will be beneficial for the design and rationalization of the practical diesel catalysts.

2. Results and Discussion

2.1. Structure and Morphology

Figure 1 shows the XRD patterns of ZSM-5, Cu/ZSM-5, and $CuCe_xZr_{1-x}$/ ZSM-5 (x = 0, 0.25, 0.5, 0.75 and 1). As expected, the catalysts still retain the ordered microstructure after the addition of copper, and cerium and/or zirconium because the inherent MFI structure of ZSM-5 (2θ = 7.8°, 8.7°, 24.5°, 24.9°, PDF 44-003) can be observed for all the catalysts. However, the incorporation of copper, and cerium and/or zirconium leads to a decrease of the intensity of the ZSM-5 principal diffraction peaks, which can be attributed to the higher absorption coefficient of metal compounds for X-ray radiation [15]. Crystallized CuO (2θ = 35.5°, 38.6°, PDF = 02-1041) nanoparticles are detected for the Cu/ZSM-5 catalysts. For the $CuZr_1$/ZSM-5, $CuCe_{0.25}Zr_{0.75}$/ZSM-5, $CuCe_{0.5}Zr_{0.5}$/ZSM-5, and $CuCe_{0.75}Zr_{0.25}$/ZSM-5 catalysts, no diffraction peaks for metal or metal oxide clusters were observed, indicating that the copper, zirconium, and cerium oxides are well dispersed as amorphous metal species, or aggregated into mini-crystals that are too small (<4 nm) to be detected by XRD [16]. For $CuCe_1$/ZSM-5, the observation of a small peak of CeO_2 (2θ = 28.2°, PDF = 34-0394) suggests that the extra-framework cerium is prone to agglomerating into cerium oxide clusters.
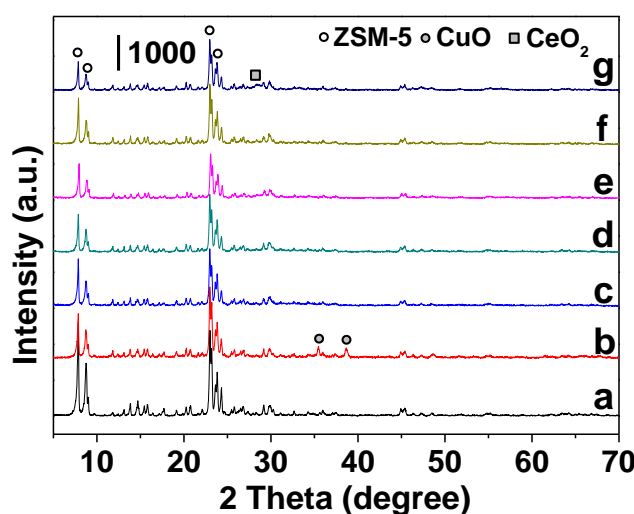

Figure 1. XRD patterns of $CuCe_xZr_{1-x}$/ZSM-5 catalysts with different loading ratios: (a) ZSM-5, (b) Cu/ZSM-5, (c) $CuZr_1$/ZSM-5, (d) $CuCe_{0.25}Zr_{0.75}$/ZSM-5, (e) $CuCe_{0.5}Zr_{0.5}$/ZSM-5, (f) $CuCe_{0.75}Zr_{0.25}$/ZSM-5, and (g) $CuCe_1$/ZSM-5.

To validate the XRD results, for each catalyst sample, more than 200 metal oxide particles from different TEM images were randomly chosen to determine the size distribution of the metal oxide particles. The size distributions of the metal oxide particles for $CuCe_{0.25}Zr_{0.75}/ZSM-5$, $CuCe_{0.5}Zr_{0.5}/ZSM-5$, $CuCe_{0.75}Zr_{0.25}/ZSM-5$, and $CuCe_1/ZSM-5$ are shown in Figure 2. The metal oxide particles in the d, e and f samples are less than 4 nm in size, while most metal oxide particles in the g sample are larger than 4 nm in size. These results are consistent with the XRD data.
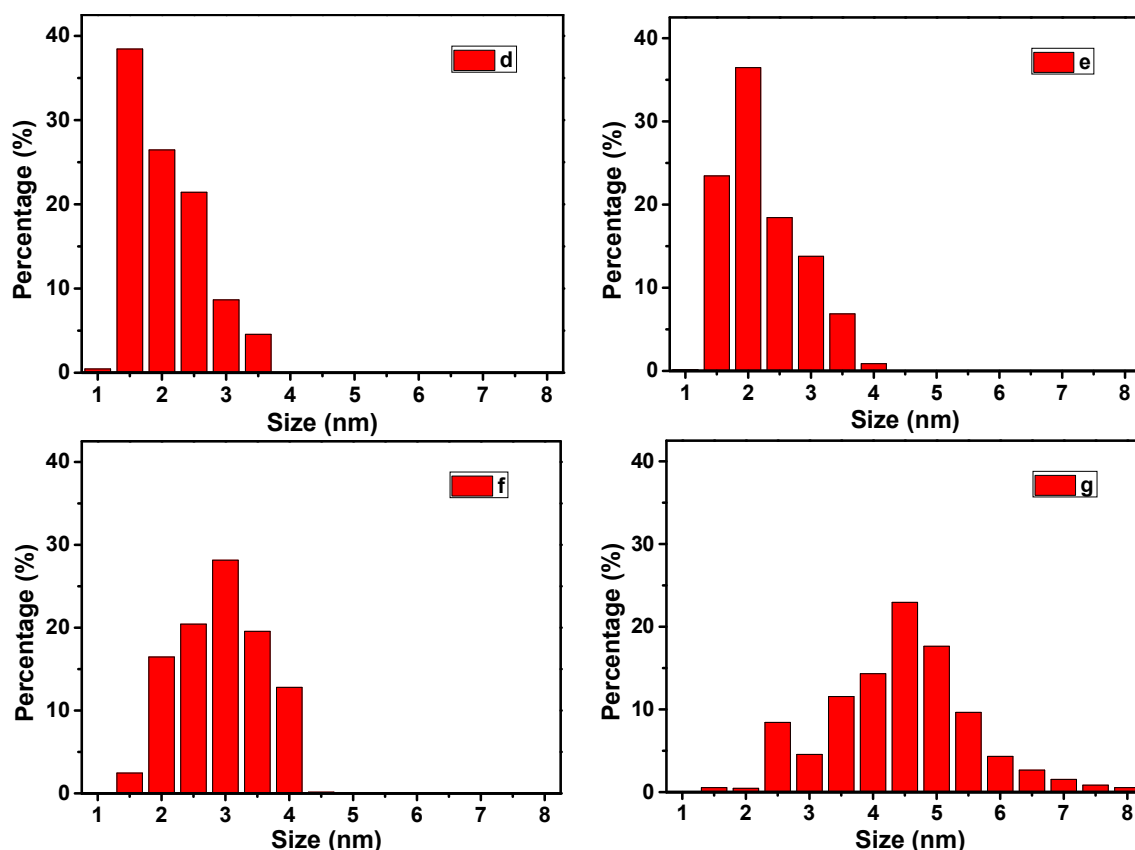
Figure 2. Size distributions of metal oxide particles for (**d**) $CuCe_{0.25}Zr_{0.75}/ZSM-5$, (**e**) $CuCe_{0.5}Zr_{0.5}/ZSM5$, (**f**) $CuCe_{0.75}Zr_{0.25}/ZSM-5$, and (**g**) $CuCe_1/ZSM-5$.

The typical TEM images of pure ZSM-5 and $CuCe_xZr_{1-x}/ZSM-5$ catalysts ($x = 0$, 0.5 and 1) are shown in Figure 3. The typical interference fringes of the ZSM-5 crystal structure are found in Figure 3a. Upon zirconium addition, small aggregates are observed for the $CuZr_1/ZSM-5$ catalyst (see Figure 3b), and most of them are less than 2 nm in size. The subsequent energy-dispersive X-ray (EDX) analysis for Point 1 in Figure 3b indicates a copper, zirconium, and oxygen-rich phase for these small aggregates. With increasing cerium content, the sizes of aggregates become larger, as shown in Figure 3c for $CuCe_{0.5}Zr_{0.5}/ZSM-5$ and Figure 3d for $CuCe_1/ZSM-5$. These results reveal that the addition of cerium decreases the dispersion of metal ions. The EDX analysis for Point 2 in Figure 3d indicates copper and cerium enrichment for the large black aggregates.
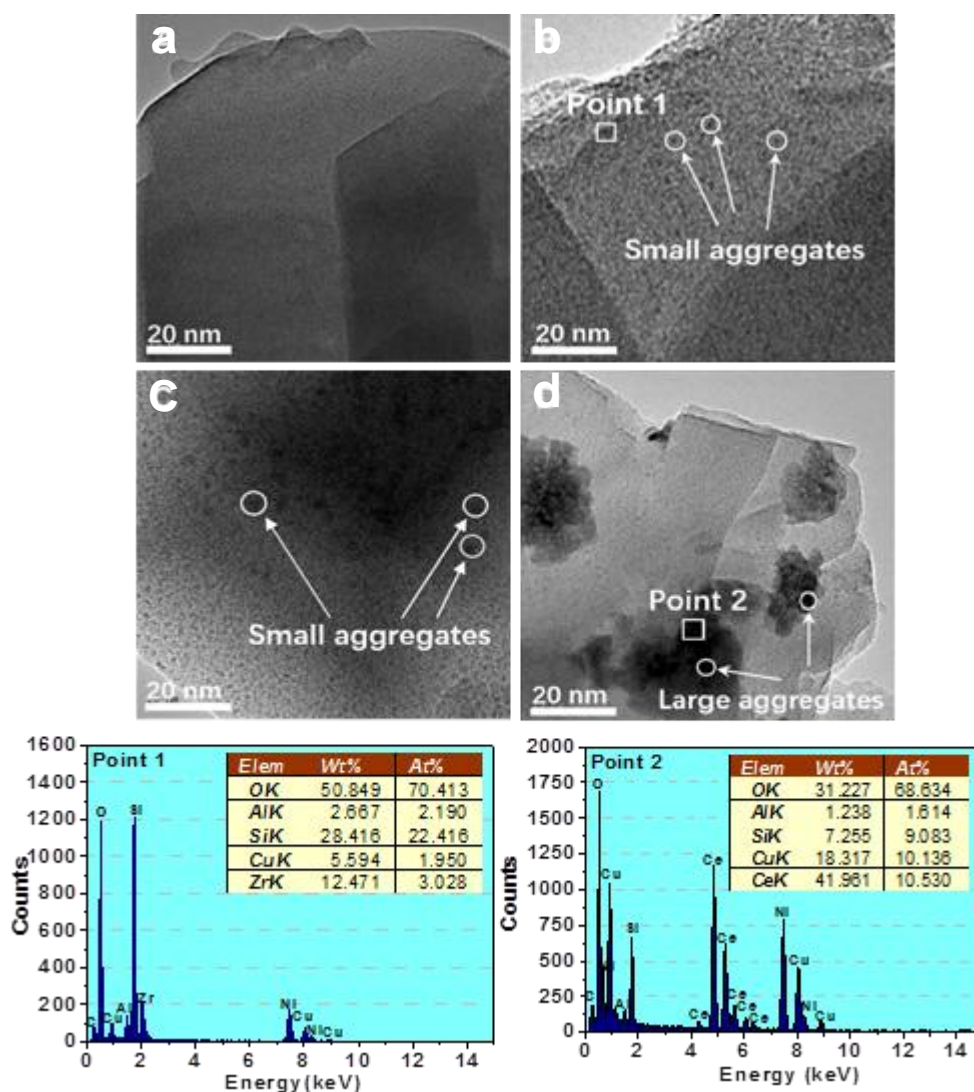
Figure 3. TEM images and energy-dispersive X-ray (EDX) quantitative analyses for (**a**) ZSM-5, (**b**) CuZr$_1$/ZSM-5, (**c**) CuCe$_{0.5}$Zr$_{0.5}$/ZSM-5, and (**d**) CuCe$_1$/ZSM-5.

2.2. XPS Analysis

The chemical state and surface composition of the elements in the catalysts were characterized by XPS. The Cu 2p spectra of the CuCe$_x$Zr$_{1-x}$/ZSM-5 catalysts (x = 0, 0.5 and 1) in Figure 4a show two main peaks: a peak at 933.3 eV that can be attributed to Cu 2p$_{3/2}$, and a peak at about 953 eV that can be attributed to Cu 2p$_{1/2}$. The intense satellite peak located at approximately 943 eV confirms the existence of divalent copper. Peak deconvolution and fitting to experimental data indicate that the Cu 2p$_{3/2}$ peak can be well fitted by two peaks at 932.5 and 933.6 eV, corresponding to the Cu$^+$ and Cu^{2+} ions, respectively [10,17,18].

The XPS spectra of O 1s for the CuCe$_x$Zr$_{1-x}$/ZSM-5 catalysts (x = 0, 0.5, and 1) in Figure 4b show two primary peaks. The peak at a higher binding energy (BE) of 531.9 eV can be assigned to regular lattice oxygen from the ZSM-5 zeolite structure [19–21], while the shoulder peak at about 529.6 eV corresponds to characteristic lattice oxygen bound to metal (copper, cerium and zirconium) cations. As the cerium content increases by 6.5% in CuCe$_1$/ZSM-5, the shoulder peak corresponding to the lattice oxygen slightly shifts to a lower BE value (529.3 eV). Considering the findings from XRD that no metal oxide crystals are observed except for the CuCe$_1$/ZSM-5 catalyst, the existence of lattice oxygen implies that the oxides are well dispersed on the ZSM-5 support as the mini-crystal form.

The XPS doublet spectra of Zr 3d obtained from the $CuCe_xZr_{1-x}$/ZSM-5 catalysts ($x = 0$ and 0.5) are shown in Figure 4c. The peaks centered at 181.9 and 184.2 eV correspond to Zr $3d_{5/2}$ and Zr $3d_{3/2}$, respectively. The BE of Zr $3d_{5/2}$ is about 0.9 eV, higher than that reported for zirconium metal and 0.5 eV lower than that reported for zirconia [22]. This phenomenon probably originates from the contribution of electrons from the surrounding species. Wang et al. [23] also found that the zirconium cations in Cu/ZrO_2 catalysts possess a lower BE of Zr $3d_{5/2}$ than zirconia, and they ascribed it to copper oxides located near oxygen vacancies on the exterior of the zirconia.

Figure 4d shows the XPS spectra of Ce 3d for the $CuCe_xZr_{1-x}$/ZSM-5 catalysts ($x = 0.5$ and 1). The complex spectrum of Ce 3d with respect to Ce $3d_{3/2}$ and Ce $3d_{5/2}$ ionization features are deconvoluted into eight components. The peaks at about 882.5, 889.3, and 898.5 eV are ascribed to the peak of Ce $3d_{5/2}$ and two "shake-up" satellite peaks, respectively. The peaks at approximately 901.1, 908.1, and 916.6 eV can be assigned to Ce $3d_{3/2}$ and two shake-up satellite peaks, respectively [9,24]. These features are viewed as the fingerprints for the existence of Ce^{4+}. The inconspicuous peaks at about 885.5 and 904.3 eV represent the initial state of Ce^{3+} [9,24]. It is evident from Figure 4d that cerium is mostly in a quadrivalent oxidation state, and a small quantity of Ce^{3+} co-exists. The presence of Ce^{3+} can be attributed to the relative homogeneous $Ce_xZr_{1-x}O_2$ or the substitution of Ce^{4+} by Zr^{4+} ions [22].
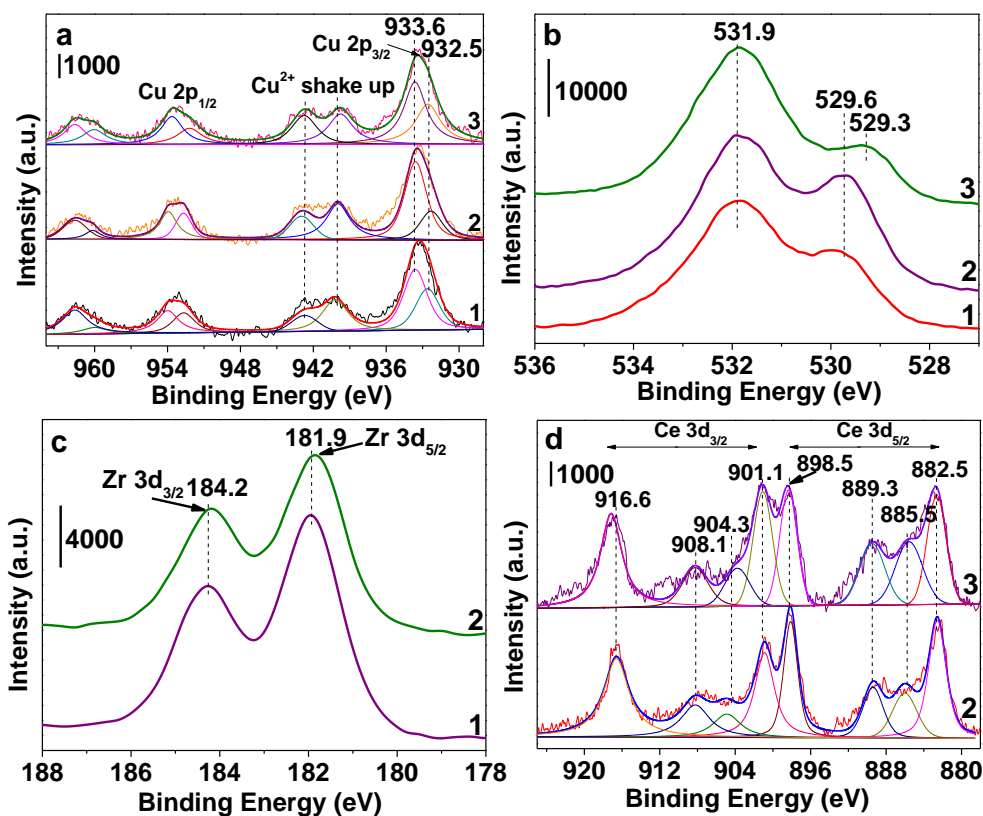
Figure 4. X-ray photoelectron spectra for (**a**) Cu 2p, (**b**) O 1s, (**c**) Zr 3d, and (**d**) Ce 3d over (1) $CuZr_1$/ZSM-5, (2) $CuCe_{0.5}Zr_{0.5}$/ZSM-5 and (3) $CuCe_1$/ZSM-5.

For the catalysts, the atomic ratios of Cu/Si, Ce/Si, and Zr/Si obtained from AAS and XPS are listed in Table 1. The atomic ratios determined from XPS are larger than those obtained from AAS, suggesting that the metal oxides become enriched on the surface of ZSM-5 grains. The atomic ratios of Cu^+/Cu^{2+} and Ce^{3+}/Ce^{4+} calculated from XPS spectra are also listed in Table 1. As the cerium content increases from 0% for $CuZr_1$/ZSM-5 to 3.4% for $CuCe_{0.5}Zr_{0.5}$/ZSM-5, the Cu^+/Cu^{2+} ratio decreases from 0.64 to 0.35, while the Ce^{3+}/Ce^{4+} ratio increases from 0 to 0.198. Upon further increasing the cerium content, the Cu^+/Cu^{2+} ratio increases to 0.71 for the $CuCe_1$/ZSM-5 catalyst, while the Ce^{3+}/Ce^{4+} ratio decreases after an initial increase.

Table 1. Surface compositions of $CuCe_xZr_{1-x}/ZSM-5$ catalysts (x = 0, 0.25, 0.5, 0.75, 1) obtained from X-ray photoelectron spectroscopy (XPS) analysis.

Sample	Cu^+/Cu^{2+}	Ce^{3+}/Ce^{4+}	Cu/Si (Atomic)		Ce/Si (Atomic)		Zr/Si (Atomic)	
			AAS	XPS	AAS	XPS	AAS	XPS
$CuZr_1/ZSM-5$	0.64	/	0.025	0.118	0	0	0.026	0.804
$CuCe_{0.25}Zr_{0.75}/ZSM-5$	0.498	0.187	0.026	0.116	0.005	0.015	0.018	0.723
$CuCe_{0.5}Zr_{0.5}/ZSM-5$	0.35	0.198	0.025	0.119	0.013	0.029	0.014	0.643
$CuCe_{0.75}Zr_{0.25}/ZSM-5$	0.672	0.298	0.024	0.117	0.020	0.034	0.007	0.312
$CuCe_1/ZSM-5$	0.71	0.247	0.026	0.116	0.025	0.066	0	0

2.3. H_2-TPR

Figure 5 shows the H_2-TPR profiles of ZrO_2, CeO_2, and the Cu/ZSM-5 and $CuCe_{0.75}Zr_{0.25}/ZSM-5$ catalysts, and the relevant data are listed in Table 2. Three main reduction peaks are evident for the catalysts: the α-peak (182–213 °C) is ascribed to the reduction of the copper species dispersed on the ZSM-5 support, the β-peak (260–264 °C) is associated with the reduction of the copper oxide adhering to the external surface of zeolite crystallites, and the γ-peak (406 °C) is generally considered to be due to the reduction of bulk and unsupported copper oxide. Some of the copper species have incorporated into the vacant sites of cerium and/or zirconium oxides to form a coordinated surface structure with capping oxygen [25], corresponding to the δ peak (164–178 °C) and the ε peak (315–342 °C). As the cerium content increases, the δ peak shifts from 171 °C for $CuZr_1/ZSM-5$ to 164 °C for $CuCe_1/ZSM-5$, indicating that the composite oxides of copper and cerium are more readily reduced than those of copper and zirconium.
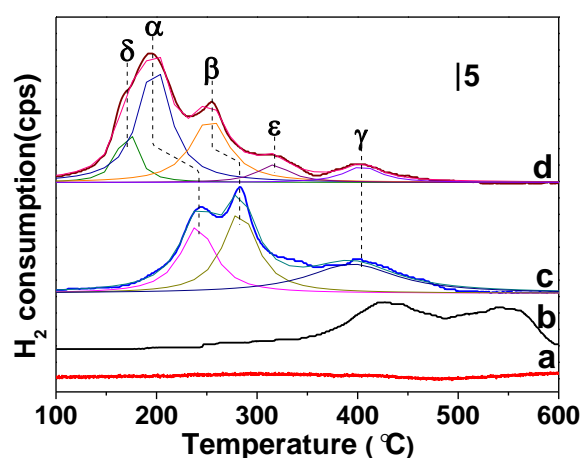
Figure 5. Temperature-programmed reduction by hydrogen (H_2-TPR) profiles of (a) ZrO_2, (b) CeO_2, (c) Cu/ZSM-5 and (d) $CuCe_{0.75}Zr_{0.25}/ZSM-5$.

Table 2. H_2-TPR results from Cu/ZSM-5 and CuCe$_x$Zr$_{1-x}$/ZSM-5 catalysts (x = 0, 0.25, 0.5, 0.75, 1).

Sample	δ Peak		α Peak		β Peak		ε Peak		γ Peak		Total H_2 Consumption (μmol/g$_{cat}$)
	T (°C)	H_2 Consumption (μmol/g$_{cat}$)	T (°C)	H_2 Consumption (μmol/g$_{cat}$)	T (°C)	H_2 Consumption (μmol/g$_{cat}$)	T (°C)	H_2 Consumption (μmol/g$_{cat}$)	T (°C)	H_2 Consumption (μmol/g$_{cat}$)	
Cu/ZSM-5	/	/	236	56.4	278	68.23	/	/	393	63.96	188.59
CuZr$_1$/ZSM-5	171	15.49	198	45.06	261	76.22	342	25.12	398	28.53	190.42
CuCe$_{0.25}$Zr$_{0.75}$/ZSM-5	175	16.92	209	66.36	259	68.49	332	17.51	407	23.54	192.82
CuCe$_{0.5}$Zr$_{0.5}$/ZSM-5	178	22.49	213	91.39	263	61.40	338	3.24	399	18.66	197.18
CuCe$_{0.75}$Z$_{0.25}$/ZSM-5	170	24.97	192	91.07	255	58.10	315	14.16	402	14.09	202.39
CuCe$_1$/ZSM-5	164	18.55	182	67.15	260	82.83	322	10.37	405	23.33	202.23

From the H_2-TPR quantitative data in Table 2, it can be seen that as the cerium content increases from 0% for $CuZr_1$/ZSM-5 to 5.2% for $CuCe_{0.75}Zr_{0.25}$/ZSM-5, the hydrogen consumption for the δ and α peak monotonously increases, while the hydrogen consumption for the β and γ peak gradually decreases. As mentioned above, the δ and α peak are related to highly dispersed copper species. Therefore, this increase in hydrogen consumption for the δ and α peak indicates that the addition of cerium improves the copper dispersion. For the $CuCe_1$/ZSM-5 catalyst, although the reduction temperatures of the δ and α peaks are lower than those for the other catalysts, the H_2 consumption of the δ and α peaks is not the maximum. This can be attributed to the formation of ceria, which is evidenced by the above XRD and TEM results. The ceria formed over the catalyst leads to the reduction not only extending deeply into the bulk of crystalline ceria but also being confined to its surface, so that the $CuCe_1$/ZSM-5 catalyst may consume less hydrogen than the $CuCe_{0.75}Zr_{0.25}$/ZSM-5 catalyst. Moreover, because the total H_2 consumption shows an increase with the cerium content increasing from 0% ($CuZr_1$/ZSM-5) to 5.2% ($CuCe_{0.75}Zr_{0.25}$/ZSM-5), the hydrogen uptake can be attributed not only to the copper reduction but also to a partial reduction of the cerium surface for the cerium-containing catalysts.

2.4. Catalytic Activity Test

Figure 5 shows the NO conversion in the SCR reaction on all the catalysts from 50 to 600 °C. All of the catalysts exhibit excellent SCR activity. For the Cu/ZSM-5 catalyst, the temperature range for 95% NO conversion is 209–406 °C. After the addition of cerium and/or zirconium to Cu/ZSM-5, the temperature range for 95% NO conversion extends toward both lower and higher temperatures, corresponding to active window broadening. The temperature ranges for 95% NO conversion are 190–436 °C for the $CuZr_1$/ZSM-5, 202–456 °C for $CuCe_{0.25}Zr_{0.75}$/ZSM-5, 203–460 °C for $CuCe_{0.5}Zr_{0.5}$/ZSM-5, 175–468 °C for $CuCe_{0.75}Zr_{0.25}$/ZSM-5, and 179–435 °C for $CuCe_1$/ZSM-5. Among the catalysts tested, the $CuCe_{0.75}Zr_{0.25}$/ZSM-5 catalyst has the highest catalytic activity for NO conversion. The improvements in the SCR activity after the addition of cerium and/or zirconium can be accounted for by three factors:

(1) The active copper species are well dispersed on the surface of the catalysts. The XRD and TEM results show that the introduction of zirconium promotes surface copper enrichment and prevents copper crystallization.

(2) The addition of cerium results in high Cu^+/Cu^{2+} ratios, as evidenced from the XPS results. In the SCR reaction, NO preferentially chemisorbs on Cu^+, and the formation of intermediate Cu^+–NO adsorbed sites is crucial for the activation of the NO molecule [26,27]. Thus, a high percentage of Cu^+ species favors catalytic NO reduction.

(3) Partial substitution of cerium and zirconium ions by copper ions contributes to the formation of copper/cerium or copper/zirconium composite oxides. As shown in the H_2-TPR experiment, these composite oxides greatly increase the reactive lattice oxygen content and reducibility, and thus improve the low-temperature activity [11].

Furthermore, as the temperature increases from 406 to 600 °C, a clear decrease of NO conversion for all the tested catalysts is observed in Figure 6. This decrease is mainly due to the occurrence of non-selective NH_3 oxidation by the reaction $4NH_3 + 5O_2 \rightarrow 4NO + 6H_2O$ at high temperatures [28–30]. The consumption of NH_3, together with the production of new NO, limits NO conversion.

The SCR process induced by all the catalysts inevitably produces N_2O and NO_2 as byproducts. In the whole temperature range considered in this study, the NO_2 concentration is below 3 ppm for all the catalysts (not shown). Figure 7 shows the yield of N_2O plotted against reaction temperature. For all the catalysts, the yield of N_2O increases with increasing temperature up until a certain temperature and then starts to decrease. The N_2O produced in the low temperature range mainly arises from side reactions between NO and NH_3: $4NO + 4NH_3 + 3O_2 \rightarrow 4N_2O + 6H_2O$ [28,29]. Upon further increase of the reaction temperature, the formation of N_2O is mainly from NH_3 oxidation via the

reaction $2NH_3 + 2O_2 \rightarrow N_2O + 3H_2O$ [28,30], and the amount of N_2O rapidly increases with the maximum yield at reaction temperatures <450 °C. In the high temperature range, non-selective NH_3 oxidation takes place by the reaction $4NH_3 + 5O_2 \rightarrow 4NO + 6H_2O$ [28–30], and thus the amount of N_2O rapidly decreases as the temperature increases. Moreover, close inspection of Figure 7 shows that the zirconium-containing catalysts yield less N_2O than the Cu/ZSM-5 and $CuCe_1$/ZSM-5 catalysts, which means that the introduction of zirconium abates N_2O formation in the tested temperature range.
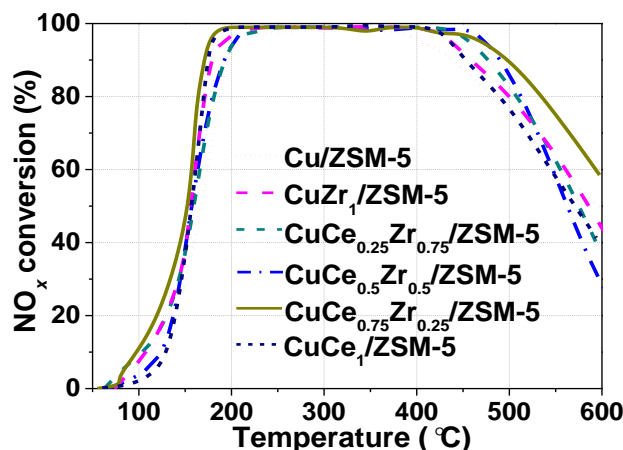
Figure 6. Catalytic activities for NO_x reduction by NH_3 for Cu/ZSM-5 and $CuCe_xZr_{1-x}$/ZSM-5 catalysts (x = 0, 0.25, 0.5, 0.75 and 1).
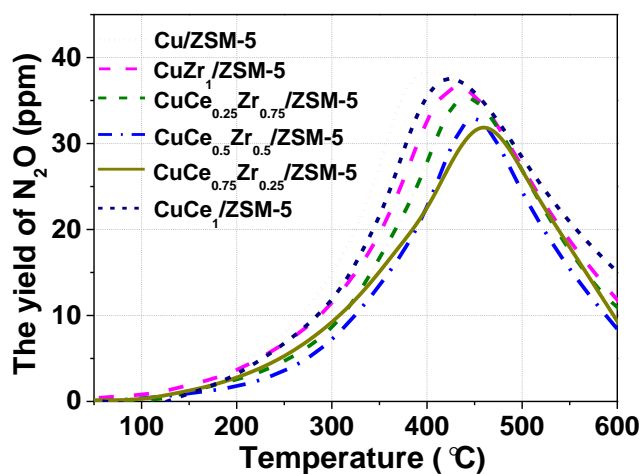
Figure 7. Yield of N_2O during the selective catalytic reduction (SCR) process as a function of reaction temperature for Cu/ZSM-5 and $CuCe_xZr_{1-x}$/ZSM-5 catalysts (x = 0, 0.25, 0.5, 0.75 and 1).

3. Experimental

3.1. Synthesis of Catalysts

H/ZSM-5 with an atomic Si/Al ratio of 25 was provided by Nankai University, Tianjin, China. A series of $CuCe_xZr_{1-x}O_y$/ZSM-5 catalysts (x = 0, 0.25, 0.5, 0.75, and 1) were synthesized by an aqueous ion-exchange technique. A desired amount of copper acetate, and zirconium and cerium nitrate was added to deionized water and mixed with 20 g of H/ZSM-5 powder at room temperature. The resulting solution was stirred at 80 °C for 24 h. The samples were filtered and dried by evaporation in air and then calcined at 550 °C for 4 h. The copper content of the $CuCe_xZr_{1-x}O_y$/ZSM-5 catalysts was fixed at 3 wt. %, and the molar ratio of Cu/(Ce + Zr) was 1:1. These catalysts are denoted as $CuZr_1$/ZSM-5, $CuCe_{0.25}Zr_{0.75}$/ZSM-5, $CuCe_{0.5}Zr_{0.5}$/ZSM-5, $CuCe_{0.75}Zr_{0.25}$/ZSM-5, and $CuCe_1$/ZSM-5. The copper,

cerium, and zirconium contents of each calcined catalyst were determined by atomic absorption spectroscopy (AAS) using a PerkinElmer AAnalyst 300 spectrometer, and the results are shown in Table 3. To evaluate the catalytic activity, the catalysts were compressed by a pressure of 20 MPa, then granulated and screened to the size of a 20–40 mesh.

Table 3. Element compositions of all catalysts.

Sample	Element Composition Measured by AAS (wt. %)			
	Cu	Ce	Zr	Si
$CuZr_1/ZSM$-5	3.0	0	4.4	52.4
$CuCe_{0.25}Zr_{0.75}/ZSM$-5	3.1	1.3	3.1	52.2
$CuCe_{0.5}Zr_{0.5}/ZSM$-5	2.9	3.4	2.3	52.3
$CuCe_{0.75}Zr_{0.25}/ZSM$-5	2.8	5.2	1.2	52.4
$CuCe_1/ZSM$-5	3.1	6.5	0	52.2

3.2. Characterization

Powder X-ray diffraction (XRD) was performed using a Rigaku D/MAC/max 2500 v/pc instrument with Cu Kα radiation (40 kV, 200 mA, λ = 1.5418 Å) (Jananese Science, Tokyo, Japan). The scan was performed with a 2θ rate of 0.02°/min from 5–80°. Transmission electron microscopy (TEM) images of the catalysts were obtained using a Philips Tecnai G2 F20 microscope operating at 200 kV equipped with an Oxford-1NCA energy-dispersive X-ray detector (EDX) (FEI, Hillsboro, OR, USA). Prior to measurement, the catalysts were dispersed in pure ethanol through sonication, and then mounted on nickel grids with a carbon film. X-ray photoelectron spectroscopy (XPS) was recorded using a Perkin-Elmer PHI-1600 ESCA spectrometer with a Mg Kα X-ray source (Perkin Elmer, Wellesley, MA, USA). The binding energies (BEs) were calibrated by referencing the C 1s at 284.8 eV. A ChemBet Pulsar system was used to perform temperature-programmed reduction by hydrogen (H_2-TPR) (Quantachrome Instruments, Boynton Beach, FL, USA). For the H_2-TPR experiments, 100 mg of the catalyst was exposed to pure Ar at a flow rate of 30 mL/min for 1 h at 300 °C. Then, the same gas was used to cool the catalyst down to 50 °C. The H_2-TPR measurements were carried out by increasing the temperature to 700 °C at a heating rate of 10 °C/min in 5% hydrogen at a constant flow rate of 30 mL/min. The hydrogen consumption was monitored and quantified using a thermal conductivity detector.

3.3. Catalytic Activity

The activities of the catalysts were measured in a continuous flow apparatus at atmosphere pressure. Before each test run, the catalyst powder was first pressed into a wafer and sieved into 20–40 meshes, and then 0.5 g of catalyst was set into a fix-bed reactor made of a quartz tube with an internal diameter of 10 mm. The reaction was carried out in the temperature range 50–600 °C, and a K-type thermocouple was located inside the catalyst bed to monitor the reaction temperature. The feed gas was controlled by calibrated electronic mass flow controllers, and contained 1000 ppm NO, 1000 ppm NH_3, and 10% O_2 and N_2 as the balance gas. The space velocity was set at 15,000 h^{-1}. An online mass spectrometry (Dycor LC-D200) was used to monitor the effluent NO, NO_2, N_2O, and NH_3. From the concentration of the gases at steady state, the NO_x conversion was defined as:

$$NO_x \text{ conversion (\%)} = \frac{[NO_x]_{in} - [NO_x]_{out}}{[NO_x]_{in}} \times 100, \ [NOx] = [NO] + [NO_2]$$

4. Conclusions

The present study has highlighted the effects of cerium and/or zirconium incorporation into Cu/ZSM-5 on the SCR activity in NO abatement. The $CuCe_xZr_{1-x}O_y/ZSM$-5 catalysts used in

this study present a more than 95% NO conversion rate in a wide temperature range (175–468 °C), which is an improvement relative to the Cu/ZSM-5 catalyst (209–406 °C) in terms of SCR activity. The zirconium doping improves copper dispersion, and the introduction of zirconium promotes surface copper enrichment and prevents copper crystallization, which favors catalytic NO reduction. Partial substitution of cerium and zirconium ions by copper ions increases the reactive lattice oxygen content and reducibility, and thus improves the low-temperature activity. Because of the existence of the Ce^{3+}/Ce^{4+} redox couple in the cerium-containing catalysts, the SCR activities of cerium-rich catalysts are higher than those of zirconium-rich catalysts. Moreover, formation of N_2O is suppressed in the range of test temperatures due to the presence of zirconium in the catalysts.

Author Contributions: This study was conducted through contributions of all authors. C.S. and G.L. designed the study and wrote the manuscript. Y.L., C.F. and X.L. designed and performed the experiments and analyzed the data. Y.L. checked and corrected the manuscript.

Conflicts of Interest: The authors declare no conflict of interest.

References

1. Landi, G.; Lisi, L.; Pirone, R.; Russo, G.; Tortorelli, M. Effect of water on NO adsorption over Cu-ZSM-5 based catalysts. *Catal. Today* **2012**, *191*, 138–141. [CrossRef]
2. Ji, Y.; Yang, H.; Yan, W. Strategies to enhance the catalytic performance of ZSM-5 zeolite in hydrocarbon cracking: A review. *Catalysts* **2017**, *7*, 367. [CrossRef]
3. Wang, T.; Wan, Z.; Yang, X.; Zhang, X.; Niu, X.; Sun, B. Promotional effect of iron modification on the catalytic properties of Mn-Fe/ZSM-5 catalysts in the Fast SCR reaction. *Fuel Process. Technol.* **2018**, *169*, 112–121. [CrossRef]
4. Xu, W.J.; Zhang, G.X.; Chen, H.W.; Zhang, G.M.; Han, Y.; Chang, Y.C.; Gong, P. Mn/beta and Mn/ZSM-5 for the low-temperature selective catalytic reduction of NO with ammonia: Effect of manganese precursors. *Chin. J. Catal.* **2018**, *39*, 118–127. [CrossRef]
5. De Lucas, A.; Valverde, J.L.; Dorado, F.; Romero, A.; Asencio, I. Influence of the ion exchanged metal (Cu, Co, Ni and Mn) on the selective catalytic reduction of NO_x over mordenite and ZSM-5. *J. Mol. Catal.* **2005**, *225*, 47–58. [CrossRef]
6. Ma, T.; Imai, H.; Yamawaki, M.; Terasaka, K.; Li, X. Selective synthesis of gasoline-ranged hydrocarbons from syngas over hybrid catalyst consisting of metal-loaded ZSM-5 coupled with copper-zinc oxide. *Catalysts* **2014**, *4*, 116–128. [CrossRef]
7. Abu-Zied, B.M.; Schwieger, W.; Unger, A. Nitrous oxide decomposition over transition metal exchanged ZSM-5 zeolites prepared by the solid-state ion-exchange method. *Appl. Catal. B* **2008**, *84*, 277–288. [CrossRef]
8. Chen, P.; Simböck, J.; Schönebaum, S.; Rauch, D.; Simons, T.; Palkovits, R.; Simon, U. Monitoring NH_3 storage and conversion in Cu-ZSM-5 and Cu-SAPO-34 catalysts for NH_3-SCR by simultaneous impedance and DRIFT spectroscopy. *Sens. Actuators B* **2016**, *236*, 1075–1082. [CrossRef]
9. Jiang, L.; Zhu, H.; Razzaq, R.; Zhu, M.; Li, C.; Li, Z. Effect of zirconium addition on the structure and properties of CuO/CeO_2 catalysts for high-temperature water-gas shift in an IGCC system. *Int. J. Hydrogen Energy* **2012**, *37*, 15914–15924. [CrossRef]
10. Seo, C.K.; Choi, B.; Kim, H.; Lee, C.H.; Lee, C.B. Effect of ZrO_2 addition on de-NO_x performance of Cu-ZSM-5 for SCR catalyst. *Chem. Eng. J.* **2012**, *191*, 331–340. [CrossRef]
11. Zhang, R.; Teoh, W.Y.; Amal, R.; Chen, B.; Kaliaguine, S. Catalytic reduction of NO by CO over $Cu/Ce_xZr_{1-x}O_2$ prepared by flame synthesis. *J. Catal.* **2010**, *272*, 210–219. [CrossRef]
12. Fu, M.; Yue, X.; Ye, D.; Ouyang, J.; Huang, B.; Wu, J.; Liang, H. Soot oxidation via CuO doped CeO_2 catalysts prepared using coprecipitation and citrate acid complex-combustion synthesis. *Catal. Today* **2010**, *153*, 125–132. [CrossRef]
13. Łamacz, A.; Krztoń, A.; Djéga-Mariadassou, G. Catalytic decomposition of nitrogen oxides from coal combustion flue gases on $CeZrO_2$ supported Cu catalysts. *Catal. Today* **2011**, *176*, 126–130. [CrossRef]

14. Si, R.; Zhang, Y.W.; Li, S.J.; Lin, B.X.; Yan, C.H. Urea-Based Hydrothermally derived homogeneous nanostructured $Ce_{1-x}Zr_xO_2$ ($x = 0-0.8$) solid solutions: A strong correlation between oxygen storage capacity and lattice strain. *J. Phys. Chem. B* **2004**, *108*, 12481–12488. [CrossRef]

15. Qi, G.; Yang, R.T. Selective catalytic oxidation (SCO) of ammonia to nitrogen over Fe/ZSM-5 catalysts. *Appl. Catal. A* **2005**, *287*, 25–33. [CrossRef]

16. Ohtsuka, H.; Tabata, T.; Okada, O.; Sabatino, L.M.; Bellussi, G. A study on selective reduction of NO_x by propane on Co-Beta. *Catal. Lett.* **1997**, *44*, 265–270. [CrossRef]

17. Oliveira, M.L.M.; Silva, C.M.; Moreno-Tost, R.; Farias, T.L.; Jiménez-López, A.; Rodríguez-Castellón, E. A study of copper-exchanged mordenite natural and ZSM-5 zeolites as SCR-NO_x catalysts for diesel road vehicles: Simulation by neural networks approach. *Appl. Catal. B* **2009**, *88*, 420–429. [CrossRef]

18. Jones, S.D.; Neal, L.M.; Everett, M.L.; Hoflund, G.B.; Hagelin-Weaver, H.E. Characterization of ZrO_2-promoted Cu/ZnO/nano-Al_2O_3 methanol steam reforming catalysts. *Appl. Surf. Sci.* **2010**, *256*, 7345–7353. [CrossRef]

19. Correa, C.M.; Castrillón, F.C. Supported bimetallic Pd-Co catalysts: characterization and catalytic activity. *J. Mol. Catal. A Chem.* **2005**, *228*, 267–273. [CrossRef]

20. Wu, Z.; Jin, R.; Liu, Y.; Wang, H. Ceria modified MnO_x/TiO_2 as a superior catalyst for NO reduction with NH_3 at low-temperature. *Catal. Commun.* **2008**, *9*, 2217–2220. [CrossRef]

21. Hwang, I.C.; Kim, D.H.; Woo, S.I. Role of oxygen on NO_x SCR catalyzed over Cu/ZSM-5 studied by FTIR, TPD, XPS and micropulse reaction. *Catal. Today* **1998**, *44*, 47–55. [CrossRef]

22. Liu, L.; Yao, Z.; Liu, B.; Dong, L. Correlation of structural characteristics with catalytic performance of $CuO/Ce_xZr_{1-x}O_2$ catalysts for NO reduction by CO. *J. Catal.* **2010**, *275*, 45–60. [CrossRef]

23. Wang, L.C.; Liu, Q.; Chen, M.; Liu, Y.M.; Cao, Y.; He, H.Y.; Fan, K.N. Structural evolution and catalytic properties of nanostructured Cu/ZrO_2 catalysts prepared by oxalate gel-coprecipitation technique. *J. Phys. Chem. C* **2007**, *111*, 16549–16557. [CrossRef]

24. Nelson, A.E.; Schulz, K.H. Surface chemistry and microstructural analysis of $Ce_xZr_{1-x}O_{2-y}$ model catalyst surfaces. *Appl. Surf. Sci.* **2003**, *210*, 206–221. [CrossRef]

25. Deo, G.; Wachs, I.E. Reactivity of supported vanadium oxide catalysts: The partial oxidation of methanol. *J. Catal.* **1994**, *146*, 323–334. [CrossRef]

26. Ansell, G.; Diwell, A.; Golunski, S.; Hayes, J.; Rajaram, R.; Truex, T.; Walker, A. Mechanism of the lean NO_x reaction over Cu/ZSM-5. *Appl. Catal. B.* **1993**, *2*, 81–100. [CrossRef]

27. Curtin, T.; Grange, P.; Delmon, B. The effect of pretreatments on different copper exchanged ZSM-5 for the decomposition of NO. *Catal. Today* **1997**, *36*, 57–64. [CrossRef]

28. Liu, Q.; Liu, Z.; Li, C. Adsorption and activation of NH_3 during selective catalytic reduction of NO by NH_3. *Chin. J. Catal.* **2006**, *27*, 636–646. [CrossRef]

29. Koebel, M.; Elsener, M.; Madia, G. Reaction pathways in the selective catalytic reduction process with NO and NO_2 at low temperatures. *Ind. Eng. Chem. Res.* **2001**, *40*, 52–59. [CrossRef]

30. Sirdeshpande, A.R.; Lighty, J.S. Kinetics of the selective catalytic reduction of NO with NH_3 over CuO/γ-Al_2O_3. *Ind. Eng. Chem. Res.* **2000**, *39*, 1781–1787. [CrossRef]